A Novel Approach Based on Simulated Annealing Coupled to Artificial Neural Network for 3-D Electric-Field Optimization

Abhijit Lahiri and Sivaji Chakravorti, *Senior Member, IEEE*

***Abstract*—This paper deals with the optimization of stress distribution on and around electrode-spacer arrangements for ensuring economical and higher reliability of gas-insulated systems. The optimization technique adopted in this paper is the artificial neural network-aided simulated-annealing (SA) algorithm. By coupling a trained neural net with the annealing algorithm, the execution speed of the latter is greatly enhanced to evaluate the optimum values for the design parameters of the electrode-spacer arrangements compared to calculating the cost function via the entire process for field calculation at every move of the optimization algorithm. The convergence of the optimization algorithm has also been compared statistically with the genetic algorithm. The results presented in this paper show that optimized electrode-spacer contours have been obtained with an acceptable degree of accuracy using the neural-network-aided SA algorithm. The statistical analysis shows a promising result for the proposed method.**

***Index Terms*—Artificial neural network (ANN), indirect boundary element method (BEM), optimization of three-dimensional (3-D) electric field, simulated annealing (SA).**

NOMENCLATURE

ANN	Artificial neural network.
BEM	Boundary element method.
GA	Genetic algorithm.
GIS	Gas-insulated system.
HJA	Hooke–Jeeves' Algorithm.
MAE	Mean absolute error.
RMSE	Root mean squared error.
SAA	Simulated-annealing algorithm.
TCF	Temperature cooling factor.
TS	Tabu search.

I. INTRODUCTION

FROM THE consideration of cost-effective design, it is preferable to have optimized electrode and insulator profiles, particularly with reference to extra high voltage systems, where the cost of insulation is prohibitively high.

Manuscript received June 24, 2003; revised August 18, 2004. The work of A. Lahiri was supported by the Council of Scientific and Industrial Research (India) in which a Senior Research Fellowship was awarded under Award 9/96(306)/98-EMR-I. The work of S. Chakravorti was supported by the All India Council for Technical Education under Project "An Integrated Method for 3D Insulation System Optimization Using Parametric CAD Module," under Grant 8019/RDII/R&D/ELE (181)/2000-01. Paper no. TPWRD-00326-2003.

A. Lahiri is with the Department of Electrical Engineering, Calcutta Institute of Engineering and Management, Kolkata 700 040, India (e-mail: jit_lahiri@yahoo.com).

S. Chakravorti is with the Department of Electrical Engineering, Jadavpur University, Kolkata 700 032, India (e-mail: s_chakravorti@ieee.org).

Digital Object Identifier 10.1109/TPWRD.2004.843457

During the past years, notable success has been achieved in applying methods based on artificial intelligence for the design, maintenance, and optimization of systems. In many cases, methods based on artificial intelligence have proven to be more efficient and a faster means of solving problems when compared to methods based on classical approaches [1]–[3].

Considerable effort has been given on the optimization of electrode-spacer configurations as reported in the literature. Electrode and insulator contours have been optimized by Singer and Grafoner [4] as well as Stih [5] using methods based on classical approaches.

Abdel-Salam [6] developed a method that modifies the profile of high-voltage insulators to obtain a uniform distribution of the tangential field along the insulator surface. To achieve the desired accuracy of the design by [4]–[6], considerable effort and time are required. Electrode contours in parallel disc have been optimized by Chakravorti [7] with a view toward obtaining an electrode contour having uniform stress distribution along the contour surface. Bhattacharya *et al.* optimized the design of toroidal electrodes [8] and also the contour of axisymmetric insulators in multidielectric arrangements [9] by artificial neural networks (ANNs) to obtain the desired electric stress distribution along the insulator surface. Mukherjee *et al.* [10] reported ANN-based optimization of a single-phase gas-insulated-system (GIS) bus termination and of the shield ring of a transformer.

Methods proposed in [7]–[10] suffer a major drawback in the sense that a trained ANN will calculate either electric stress for a given set of design parameters or the design parameters for a desired output. Optimum contours are not available from the entire search space of each of the design parameters from [7]–[10]. To overcome such problems and to increase the precision and efficiency of designing optimum electrode-spacer contours, an alternative method has been proposed in this paper.

Here, an accelerated algorithm is presented for optimizing the three-dimensional (3-D) electric field using an ANN-aided simulated-annealing algorithm (SAA). An input–output data set was prepared by means of electric-field calculations using the indirect boundary element method (BEM) [11] for training the neural network. This was done by varying those design parameters that affect the resultant field distribution along the respective insulator surfaces significantly.

The purpose of incorporating a trained neural network is that when the SAA executes, then the trained ANN calculates the cost function (i.e., electric stress for a given set of design parameters, instead of electric-field calculations). These electric stresses, in turn, are returned to the SAA to decide upon the

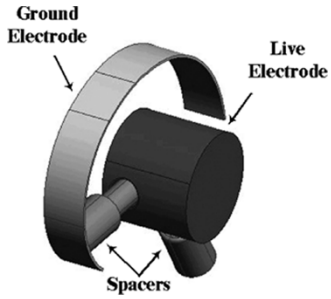

Fig. 1. Electrode-spacer arrangement of application example 1.

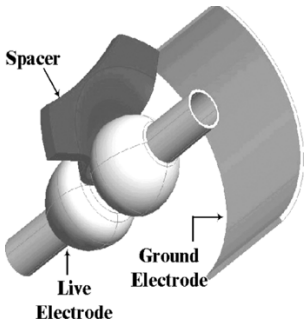

Fig. 2. Electrode-spacer arrangement of application example 2.

convergence of the latter. This coupled processing of an SAA and an ANN significantly enhances the speed of optimizing the 3-D electric field.

II. Application Examples

Figs. 1 and 2 show the two electrode-spacer arrangements that were considered as application examples. In each of these arrangements, the electrodes are of extruded aluminum with the inner electrode being the live electrode, which is maintained at a potential of 1 V (normalized voltage for ready reference), and the outer cylindrical enclosure is maintained at ground potential.

The insulators are of epoxy cast resin with a relative permittivity of 5.3 and the gaseous dielectric is a mixture of SF_6/N_2 [12] with a relative permittivity of 1.005.

III. Electric-Field Distribution on and Around 3-D Electrode-Spacer Arrangements

Indirect BEM [13] was applied to calculate the electric-field distribution. The procedural steps in such an electric-field calculation are shown in Fig. 3.

Equivalent surface charges are introduced along the discrete boundary elements in such a way that they satisfy the prescribed boundary conditions on the conductor surfaces as well as on the dielectric–dielectric boundaries [14]. For each of the two examples considered, the results are presented primarily for insulator surfaces, since the study is aimed at getting an optimized field along the insulator surfaces.

Fig. 4 shows the generated mesh over part of the live electrode that is projected inward. Fig. 5 presents the mesh generated on one of the insulator surfaces for application example 1. For the purpose of optimizing the electric field along the insulator surface of application example 1, the following parameters are varied:

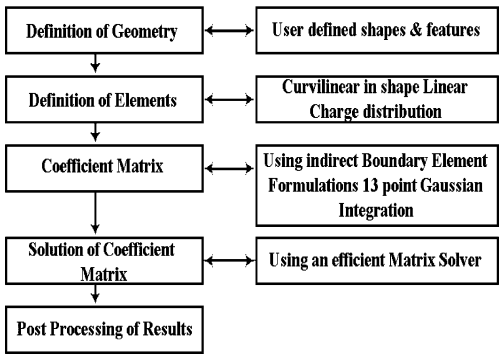

Fig. 3. Procedural steps in electric-field calculation.

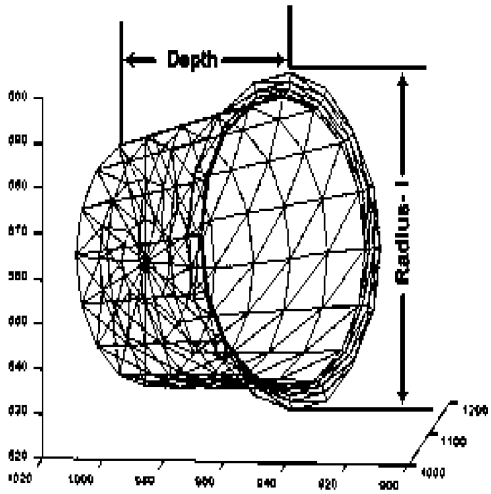

Fig. 4. Part of the live electrode of example 1 projected inward.

- radius-I (Rad-I), as indicated in Fig. 4;
- span of the section indicated by Section III in Fig. 5;
- insertion depth of the part of the live electrode shown by depth in Fig. 4.

Fig. 6 shows the generated mesh over the insulator surface of application example 2. Fig. 7 shows the generated mesh over the live electrode. To optimize the electric field along the insulator surface, the radii are varied for the spacer section as indicated by Section II in Fig. 6, and the sections of the live electrode referred as Sections I and III, respectively, in Fig. 7.

These parameters are chosen in the respective examples based on exploratory computations that show a significant effect on the field distribution along the insulator surface. The design parameters are varied over a wide range. The effects of such variations on the maximum resultant stress $E_{\mathrm{R\,max}}$ along the insulator surfaces are detailed in the following sections.

A. Effect of Variation of the Design Parameters, Example 1

First, Rad-I is varied in steps of $\pm 2.5\%$ from its initial value of 37.5 mm, keeping span and depth constant at 12° and 80 mm, respectively.

Then, keeping Rad-I and depth constant at 45 and 80 mm, respectively, span is changed in steps of $\pm 2°$ from its initial value of 12°.

Finally, with Rad-I and span constant at 45 mm and 2°, respectively, depth is decreased in steps of 2 mm from its initial

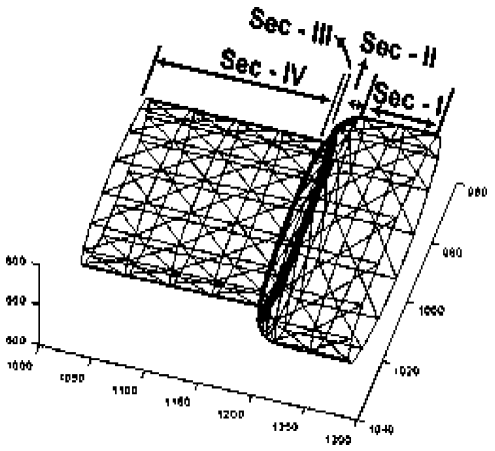

Fig. 5. One of the insulators of application example 1.

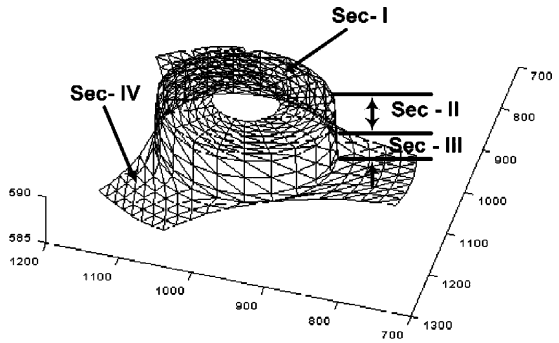

Fig. 6. Insulator of application example 2.

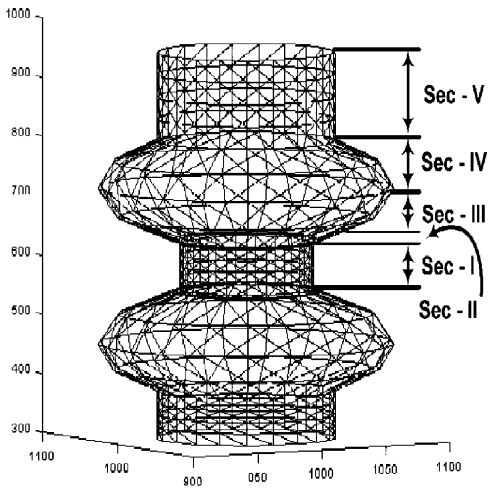

Fig. 7. Live electrode of application example 2.

value of 80 mm. Representative results for such variations in the design parameters on $E_{\mathrm{R\,max}}$ are presented in Table I.

B. Effect of Variation of the Design Parameters, Example 2

Initially, Rad-II and Rad-III (i.e., the radii of Sections I and III of the live electrode are kept constant at 45 and 100 mm, respectively, and Rad-I (i.e., the radius of Section II of the spacer surface is varied in steps of ± 0.5 mm from its initial value of 3.5 mm).

TABLE I
EFFECT OF VARIATION OF THE DESIGN PARAMETERS ON $E_{\mathrm{R\,max}}$ ALONG THE INSULATOR SURFACES

For Example 1		For Example 2	
Rad-I (mm)	E_{Rmax} (V/mm)/V	Rad-I (mm)	E_{Rmax} (V/mm)/V
35.6	0.045560	0.5	0.010029
37.5	0.023860	1.0	0.009239
44.1	0.011736	4.5	0.011715
46.1	0.015111	7.0	0.012288
Span (deg)	E_{Rmax} (V/mm)/V	Rad-II (mm)	E_{Rmax} (V/mm)/V
30	0.015499	50.5	0.008900
14	0.011887	49.0	0.008851
8	0.010702	45.5	0.009112
1	0.012001	43.0	0.009201
Depth (mm)	E_{Rmax} (V/mm)/V	Rad-III (mm)	E_{Rmax} (V/mm)/V
80	0.008540	115	0.010601
56	0.002303	95	0.008866
44	0.002127	75	0.008371
38	0.004840	65	0.008630

TABLE II
VARIATION LIMITS OF THE DESIGN OPTIMIZATION PARAMETERS

Optimization Parameters for Application Example 1		
Parameters	Lower Bound	Upper Bound
Rad–I (mm)	33.8	45.0
Span (deg)	2.0	30.0
Depth (mm)	40.0	80.0
Optimization Parameters for Application Example 2		
Parameters	Lower Bound	Upper Bound
Rad–I (mm)	1.0	7.0
Rad-II (mm)	43.0	50.0
Rad–III (mm)	70.0	115.0

In the next step, with Rad-I and Rad-III constant at 1 and 100 mm, respectively, Rad-II is varied in steps of ± 0.5 mm from its initial value of 45 mm.

Last, with Rad-I and Rad-II constant at 1 and 50 mm, respectively, Rad-III is varied in steps of ± 5 mm from its initial value of 100 mm. Table I presents results that show the effect of variation of the above parameters on $E_{\mathrm{R\,max}}$.

C. Variation Limits of the Design Parameters Chosen for Optimization

The range of variation of the design parameters in the search space of the SAA is detailed in Table II. The choice of limits for each of the design parameters is constrained by electrical and mechanical considerations for the respective electrode-spacer arrangements and is supported by the results of the field computations as reported in the previous section.

IV. MATHEMATICAL FORMULATION OF THE PROBLEM

The problem of optimization of 3-D electrostatic field within the electrical and mechanical constraint of the systems can be mathematically represented in the following manner:

$$\begin{aligned} &\text{Minimize } (E_{\mathrm{R\,max}}) = f(\text{design\_param\_}i) \\ &\qquad \text{Subject to} \\ &(\text{Lower\_limit})_{\mathrm{i}} <= \text{design\_param\_}i <= (\text{Upper\_limit})_{\mathrm{i}} \\ &\text{design\_param\_}i > 0; \quad i = 1,2,3 \end{aligned} \tag{1}$$

where $\mathrm{design\_param\_i}$ is the ith design parameter of the respective arrangements as mentioned in the first column of Table II. The objective is to minimize $E_{\mathrm{R\,max}}$ which is a function of $\mathrm{design\_param\_i}$ as represented by (1). $(\mathrm{Lower\_limit})_{\mathrm{i}}$ and $(\mathrm{Upper\_limit})_{\mathrm{i}}$ are, respectively, the lower bound and the upper bound of the ith parameter given in the second and the third column of Table II. The ith parameter is allowed to vary within these bounds in the search space of SAA.

From (1), it is seen that $E_{\mathrm{R\,max}}$ is a function of the design parameters. Furthermore, a change in any design parameter does not affect the other parameters. Hence, the design parameters are the independent variables, while $E_{\mathrm{R\,max}}$ is the dependent variable of the problem.

V. ANN Architectures

A multilayered feedforward neural network has been employed in this paper. Each of the neural networks considered for the two application examples is a three-layered structure comprised of an input layer, one hidden layer, and an output layer. These are referred to as ANN 1 and ANN 2, respectively. For the problem of contour optimization, the input–output training sets (i.e., the predetermined spacer contours and the maximum resultant stress $E_{\mathrm{R\,max}}$) along such spacers are known from the results of electric-field computations. Hence, multilayer feedforward networks with supervised learning are well suited to this problem.

The backpropagation algorithm is widely used as a supervised learning algorithm in feedforward multilayer neural networks. What makes this algorithm different from the others is the process by which the weights are calculated during the learning network.

During learning, the synaptic weights are required to be updated for which an error function must be calculated. The backpropagation algorithm can calculate the error at the hidden layers very efficiently and, hence, has gained wide acceptability. Another major strength of backpropagation algorithm is its ability to produce nonlinear solutions to ill-defined problems.

For the above reasons, the ANN simulator is trained by using a backpropagation algorithm. Since three design parameters are selected for each of the two examples under consideration, three input neurons are required in each of the ANN architectures. Respective design parameters are the input variables for the two ANNs. Since the objective is to minimize the electric field along the surface of the insulators, one output neuron is required. $E_{\mathrm{R\,max}}$ along the surface of the insulators serves as the output variable for both the ANNs.

ANN 1 was trained using 52 sets of data while ANN 2 has been trained with 41 sets of data. The number of training sets of a neural net depends on two factors:

- number of learnable parameters in the network;
- number of parameters required to describe the function.

In the present case, each net has only one learnable parameter (i.e., $E_{\mathrm{R\,max}}$) and only three parameters to describe $E_{\mathrm{R\,max}}$. Moreover, the training set has no noisy data. For these reasons, a relatively smaller number of training data was found to provide adequate training.

TABLE III
Optimum Models of ANN 1 and ANN 2

Neural Network Parameters	ANN 1	ANN 2
No. of hidden layers	1	1
No. of nodes in the hidden layer	7	7
Learning rate	0.3	0.3
Momentum constant	0.8	0.9
RMS error limit for training	0.0001	0.0005
No. of iterations	75000	55000

For the purpose of testing the accuracy of the trained ANN for interpolation, a set of six data each is considered for both of the networks. Similarly, to evaluate the performance of the trained ANN for extrapolation, a different set of six data for each of the two networks has been considered. The training and test data were generated by electrostatic-field calculation using indirect BEM formulation.

By varying the network parameters, such as number of hidden layers, number of neurons in the hidden layer, learning rate, momentum constant, and/or number of iterations, the performance of the network can be varied. There is, as such, no general rule for *a priori* selection of the combination of the parameters that will give the best result for the electric-field distribution. Both ANN 1 and ANN 2 have been applied using different combinations of parameters until the mean absolute error (MAE) for the test data as mentioned above is about 1%.

The network parameter optimization technique is based on the comparison of training and test data accuracies for different combination of parameters for a fixed number of iterations. The training accuracy is measured by root mean squared error (RMSE). The test data accuracy, on the other hand, is measured by the percentage of MAE. The expressions for both errors are reported in [7].

The optimum values obtained for each of the network parameters are presented in Table III. With these parameter values, the MAE for ANN 1 is 1.28% and that for ANN 2 is 0.15% when the test data are interpolated. When they are extrapolated, the respective MAE are 1.33% and 0.26%. These results clearly show that the training accuracy is acceptable with the selected number of patterns used during training. It also proves the efficacy of the trained ANN as a function estimator for the problem under consideration.

Hence, the ANN models trained with parameters of Table III are considered as optimum for use in ANN-aided SAA.

VI. Selection of Optimization Algorithm

The efficiency of SA [15]–[18] in arriving at the near optimal solution of complex combinatorial problems is high, implementation of the algorithm [19] is simple, and convergence to a desired optimum is faster than classical optimization approaches. SA has also certain advantages over optimization algorithms based on soft computing techniques such as the genetic algorithm (GA) and tabu search (TS).

The GA treats combinations of two existing solutions as being "near," making the assumption that a child of two good solutions is probably better than a random solution. But for a particular problem or representation, if this assumption is not true, then GA will fail to provide an advantage over SAA.

The approach with two levels of solution representation, viz. genotype and phenotype to prevent destructive crossover, has traditionally been specific to the GA. But implementation of such an idea requires a lot of effort.

If mutation is the dominant way of creating new solutions, then the GA, in fact, acts as a parallel version of the SAA, where several solutions are being independently improved. But maximization of the preservation of hyperplane samples after selection demands that mutation should perhaps not be used at all, or if used then it should be at very low levels. This makes the GA more complicated compared to the SAA that can be implemented in a straightforward way.

The basic GA does not offer any statistical guarantee of global convergence to any optimal point. The SAA employs a random search which not only accepts the changes that decrease the cost function but also some changes that increase it. The later is accepted with a probability

$$p = \exp\left(\frac{-\Delta E}{cT}\right) \tag{2}$$

where ΔE is the change in the cost function E, T is a control parameter, and c is a constant. This stochastic nature of the SAA is its greatest strength. Furthermore, when there is a strong correlation between the input parameters, SAA is reported to perform better than GA [20].

Another adaptive technique used in combinatorial optimizations is the TS method, which can be applied to different problems. But the TS offers only heuristic improvement. It does not guarantee improvement in a strict sense. There is no guaranteed convergence to a global minimum as opposed to the SAA. Because of the above reasons, the SAA is applied in the present case as an optimization algorithm.

VII. ANN-Aided SAA

The optimization technique implemented in this paper follows the Metropolis algorithm [19] for the annealing process. It calculates the cost function (i.e., $E_{\mathrm{R}\max}$) along the insulator surfaces, using a neural network trained by the results of electric-field computations.

In the SAA, a random number generator is used to generate the random changes of the control variables of the algorithm and also for the temperature-dependent acceptance test. Particularly for problems that require a large number of iterations, the random number generator should have good spectral properties. For the SAA applied here, the random number generator with the initializer seed is used. It should be mentioned that for both examples, the seed was varied over a wide range, from 1 to 127, but only the meaningful variations are reported in this paper.

An ANN-aided SAA with a cooling schedule is presented in Fig. 8. This cooling schedule developed by Krikpatric [19] is known as geometric cooling. It calculates the new temperature as

$$T_{k+1} = \alpha T_k. \tag{3}$$

Thus, multiplying by a constant factor α, termed the temperature cooling factor, the temperature of the annealing schedule

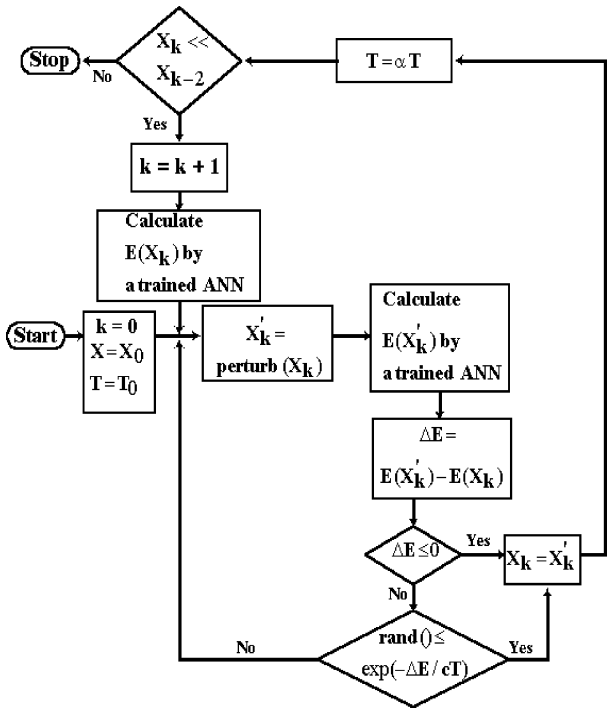

Fig. 8. Schematic diagram for ANN-aided SAA.

is regulated. However, there is a tradeoff between the temperature decrement between stages and the number of iterations per stage. For example, when the temperature is kept constant long enough to reach equilibrium, greater decrements are allowed.

The use of a trained neural network accelerates the optimization algorithm for evaluating the cost function compared to actual field computation, which requires much greater time for complete execution. The cost function evaluated through the trained neural network is returned to the SAA to decide whether it has converged or needs to proceed to the next step.

VIII. Results and Discussions

The ANN-aided SAA for minimization of $E_{\mathrm{R}\max}$ along the insulator surfaces for application examples 1 and 2 starts with the values of the control parameters of the annealing algorithm tabulated in Table IV. These are randomly chosen values used to initialize the SAA. To obtain a set of optimum design parameters for which the electric stress along the insulator surfaces is minimum, the control parameters of the SAA are varied as detailed in the following sections.

A. Sensitivity of Seed

SAA is a stochastic method of optimization. Hence, for statistical evaluation, corresponding to a particular value of seed, the maximum, average and minimum value of $E_{\mathrm{R}\max}$ obtained from the ANN-aided SAA (i.e., $E^{\mathrm{o}}_{\mathrm{R}\max}$) has been studied for both examples. The fifth column of Tables V and VII, which shows the effect of variation of seed, presents three values of $E^{\mathrm{o}}_{\mathrm{R}\max}$. The first one is the maximum value of $E^{\mathrm{o}}_{\mathrm{R}\max}$ while the second one is the average of all $E^{\mathrm{o}}_{\mathrm{R}\max}$ obtained in each temperature step during the execution of SAA and the last one

TABLE IV
INITIAL VALUES OF THE CONTROL PARAMETERS FOR SAA USED FOR APPLICATION EXAMPLES 1 AND 2

Control Parameters of SAA	Initial Values (Example 1)	Initial Values (Example 2)
Seed	40	25
Initial temperature ($T_{initial}$)	50000	50000
Maximum no. of temperature steps	700	700
Temperature cooling factor (TCF)	0.96	0.98
Number of moves	100	100
Increment or decrement factor	1	1
Upper limit of acceptance ratio	0.98	0.98
Lower limit of acceptance ratio	0.85	0.85

TABLE V
EFFECT OF VARIATION OF SEED ON OPTIMIZATION OF APPLICATION EXAMPLE 1 AND ON CORRESPONDING $E_{R\,max}$ ALONG THE SPACERS

Seed	Rad-I (mm)	Span (deg)	Depth (mm)	E^{o}_{Rmax} (V/mm)/V	E^{c}_{Rmax} (V/mm)/V
15	44.9	13.1	40.8	4.741e-4 2.673e-5 1.288e-5	1.295e-5
20	44.7	13.3	40.2	3.850e-4 2.062e-5 1.302e-5	1.308e-5
25	44.9	13.5	40.0	3.983e-4 2.121e-5 1.287e-5	1.289e-5
30	44.6	13.5	40.2	4.253e-4 2.287e-5 1.308e-5	1.312e-5
35	44.7	13.6	40.1	3.821e-4 2.530e-5 1.294e-5	1.302e-5
40	44.6	13.5	40.4	2.081e-4 3.877e-5 1.322e-5	1.331e-5
45	44.8	13.5	40.1	3.026e-4 3.888e-5 1.292e-5	1.304e-5
50	44.6	13.3	40.0	3.806e-4 3.211e-5 1.301e-5	1.321e-5
55	44.6	13.8	40.3	4.870e-4 4.327e-5 1.320e-5	1.342e-5

TABLE VI
EFFECT OF VARIATION OF TCF ON OPTIMIZATION OF APPLICATION EXAMPLE 1 AND ON CORRESPONDING $E_{R\,max}$ ALONG THE SPACERS

TCF	Rad-I (mm)	Span (deg)	Depth (mm)	E^{o}_{Rmax} (V/mm)/V	E^{c}_{Rmax} (V/mm)/V
0.90	44.8	13.6	40.2	1.299e-5	1.306e-5
0.91	44.9	13.8	40.3	1.300e-5	1.305e-5
0.92	44.8	13.7	40.2	1.297e-5	1.302e-5
0.93	44.9	13.6	40.1	1.286e-5	1.287e-5
0.94	44.8	13.5	40.2	1.299e-5	1.306e-5
0.95	44.6	13.3	40.1	1.303e-5	1.309e-5
0.96	44.9	13.5	40.0	1.287e-5	1.289e-5
0.97	44.7	13.4	40.2	1.305e-5	1.308e-5
0.98	44.2	11.8	40.1	1.342e-5	1.354e-5

is the least value of $E^{o}_{R\,max}$, (i.e., the value of $E_{R\,max}$ at which the SAA has converged).

TABLE VII
EFFECT OF VARIATION OF SEED ON OPTIMIZATION OF APPLICATION EXAMPLE 2 AND ON CORRESPONDING $E_{R\,max}$ ALONG THE SPACER

Seed	Rad-I (mm)	Rad-II (mm)	Rad-III (mm)	E^{o}_{Rmax} (V/mm)/V	E^{c}_{Rmax} (V/mm)/V
20	2.0	49.6	70.4	9.026e-3 8.042e-3 7.888e-3	7.877e-3
25	1.0	49.9	70.1	8.712e-3 7.925e-3 7.865e-3	7.866e-3
30	1.4	49.8	70.6	9.134e-3 8.538e-3 7.964e-3	7.934e-3
35	1.8	49.2	70.5	9.949e-3 8.727e-3 8.132e-3	8.152e-3
40	1.4	49.9	70.2	9.717e-3 8.228e-3 8.002e-3	8.025e-3
45	1.8	48.9	70.8	8.785e-3 7.836e-3 7.527e-3	7.878e-3

B. Effect of Variation of Seed, Example 1

First, the seed is varied in steps of ± 5 and the effect on $E_{R\,max}$ is reported in Table V, where $E^{c}_{R\,max}$ is obtained from field calculation by the indirect BEM. As shown in Table V, the best value of seed is equal to 25. Henceforth, the seed value for the SAA is 25.

C. Effect of Variation of TCF, Example 1

In the next step, with the seed kept at 25 and other control parameters of the SAA kept constant at their initial values, the TCF is varied from its initial value of 0.96. The effect of such a variation on the optimum design parameters of application example 1 and the corresponding value of $E_{R\,max}$ is presented in Table VI, from which it can be seen that the best value of TCF is 0.93.

Changes in other parameters of the SAA produce very little effect and, hence, are not reported in this paper.

D. Effect of Variation of Seed, Example 2

Keeping all other control parameters of the SAA constant, the seed is initially varied in steps of ± 5 from its initial value of 25. The resulting effect is shown in Table VII. From Table VII, the best seed value is found to be 25. So the results reported henceforth are for a seed equal to 25.

E. Effect of Variation of $T_{initial}$ and TCF, Example 2

With the seed equal to 25 and other parameters at their initial values, the initial temperature of the SAA is varied in the manner shown in Table VIII. Table VIII shows that it is best to start the annealing schedule from a temperature of 50 000.

Finally, keeping the seed equal to 25, $T_{initial}$ equal to 50 000 and all other SAA parameters constant at their preset values, the TCF is tuned in steps. The effect of such tuning is presented in Table IX, from which the best value of the TCF is found to be 0.94.

TABLE VIII
EFFECT OF VARIATION OF $T_{initial}$ ON OPTIMIZATION OF APPLICATION EXAMPLE 2 AND ON CORRESPONDING $E_{R\,max}$ ALONG THE SPACER

$T_{initial}$	Rad-I (mm)	Rad-II (mm)	Rad-III (mm)	E^{o}_{Rmax} (V/mm)/V	E^{c}_{Rmax} (V/mm)/V
60000	1.1	49.8	70.1	7.886e-3	7.898e-3
50000	1.0	49.9	70.1	7.865e-3	7.866e-3
40000	1.2	49.5	70.5	7.902e-3	7.915e-3
30000	1.2	49.2	70.8	7.913e-3	7.928e-3
20000	1.5	49.8	70.8	7.956e-3	7.972e-3
10000	1.5	48.5	71.0	7.991e-3	8.251e-3

TABLE IX
EFFECT OF VARIATION OF TCF ON OPTIMIZATION OF APPLICATION EXAMPLE 2 AND ON CORRESPONDING $E_{R\,max}$ ALONG THE SPACER

TCF	Rad-I (mm)	Rad-II (mm)	Rad-III (mm)	E^{o}_{Rmax} (V/mm)/V	E^{c}_{Rmax} (V/mm)/V
0.90	1.0	49.7	70.1	7.864e-3	7.875e-3
0.91	1.1	49.8	70.1	7.869e-3	7.882e-3
0.92	1.3	49.9	70.3	7.876e-3	7.884e-3
0.93	1.2	49.5	70.5	7.915e-3	7.923e-3
0.94	1.0	49.9	70.0	7.798e-3	7.797e-3
0.95	1.5	48.8	70.2	7.964e-3	7.985e-3
0.96	1.2	48.5	70.2	7.898e-3	7.998e-3
0.97	1.3	49.6	70.1	7.875e-3	7.877e-3
0.98	1.0	49.9	70.1	7.865e-3	7.866e-3

TABLE X
FINAL VALUES OF THE CONTROL PARAMETERS OF THE SAA THAT PRODUCE THE LEAST VALUE OF $E_{R\,max}$ ALONG THE INSULATOR SURFACES OF APPLICATION EXAMPLES 1 AND 2

Control Parameters of SAA	Final Values (Example 1)	Final Values (Example 2)
Seed	25	25
Initial temperature ($T_{initial}$)	50000	50000
Maximum no. of temperature steps	700	700
Temperature cooling factor (TCF)	0.93	0.94
Number of moves	100	100
Increment or decrement factor	1	1
Upper limit of acceptance ratio	0.98	0.98
Lower limit of acceptance ratio	0.85	0.85

Little or no effect was observed when the other control parameters of the SAA were varied for example 2. Hence, those results are not reported here.

Thus, the SAA for application examples 1 and 2 converges to produce the least value of $E_{R\,max}$ along the insulator surface when the control parameters are as shown in Table X.

F. Optimization Using Hooke–Jeeves' Algorithm (HJA)

The HJA [21] is one of the optimization methods that is based on the classical approach. It applies both direct search as well as pattern search. The control parameters of the HJA are the number of intervals, step size, acceleration factor, and acceleration factor spacing.

The HJA was applied using different combinations of the control parameters until the optimum electrode-spacer configurations were achieved. Table XI shows the optimum values of the control parameters for the HJA that produce the least value of $E_{R\,max}$ along the insulator surfaces of examples 1 and 2.

TABLE XI
OPTIMUM VALUES OF THE CONTROL PARAMETERS OF THE HJA THAT PRODUCE THE LEAST VALUE OF $E_{R\,max}$ ALONG THE INSULATOR SURFACES OF APPLICATION EXAMPLES 1 AND 2

Control Parameters of HJA	Optimum Values (Example 1)	Optimum Values (Example 2)
Number of intervals	15	25
Step size	5	5
Acceleration factor	0.01	0.01
Acceleration factor spacing	10	10

TABLE XII
OPTIMUM CONFIGURATIONS OBTAINED FROM THE SAA AND THE HJA

Application Examples	Design Parameters	Optimized values from		E^{o}_{Rmax} (V/mm)/V	
		SAA	HJA	SAA	HJA
1	Rad-I (mm)	44.9	45.0	1.286 e-5	1.300 e-5
	Span (deg)	13.6	14.0		
	Depth (mm)	40.1	40.0		
2	Rad-I (mm)	1.0	1.0	7.798 e-3	7.800 e-3
	Rad-II (mm)	49.9	49.9		
	Rad-III (mm)	70.0	70.0		

TABLE XIII
SUGGESTED OPTIMIZED CONFIGURATIONS FOR EXAMPLES 1 AND 2

Application Example	Design Parameters	Optimized Values	E^{c}_{Rmax} (V/mm)/V
1	Rad-I (mm)	45.0	1.298e-5
	Span (deg)	14.0	
	Depth (mm)	40.0	
2	Rad-I (mm)	1.0	7.796e-3
	Rad-II (mm)	50.0	
	Rad-III (mm)	70.0	

G. Optimized Configurations for Application Examples 1 and 2 Obtained From the SAA and the HJA

Optimum configurations for application examples 1 and 2 and the corresponding values of $E_{R\,max}$ are given in Table XII. These values are obtained when the values of the control parameters of the SAA and the HJA are those shown in Tables X and XI, respectively. From Table XII, it is seen that both the SAA and the HJA have converged to the same feasible solution.

From the above results, the final configurations for application examples 1 and 2, approximated to the nearest practical dimensions that will produce the minimum $E_{R\,max}$ on the respective insulator surfaces are summarized in Table XIII.

H. Explanation of Table XII

For application example 1 it is observed from Table V that, corresponding to a seed equal to 25, both $E^{o}_{R\,max}$ and $E^{c}_{R\,max}$ are least. Hence, with the seed equal to 25, TCF has been varied. From Table VI, it is observed that for TCF equal to 0.93 both $E^{o}_{R\,max}$ and $E^{c}_{R\,max}$ are least. It has also been reported that changes in other parameters of the SAA have produced insignificant effect on its convergence. Thus, it may be concluded that for a seed equal to 25 and TCF equal to 0.93, the SAA has converged to the desired least value of $E_{R\,max}$. Consequently, from Table VI, it is observed that for a TCF equal to 0.93, the SAA has converged to the values of the design parameters given in Table XII.

For example 2, it is seen from Table VII that for a seed equal to 25 $E^{\mathrm{c}}_{\mathrm{R\,max}}$ is minimum, while $E^{\mathrm{o}}_{\mathrm{R\,max}}$ is minimum for a seed equal to 45. But here, a seed value of 25 has been considered for further study. This is due to the reason that with the set of design parameters calculated by the SAA corresponding to seed value of 25, the least value of $E_{\mathrm{R\,max}}$ has been obtained from the field calculation. Hence, with a seed equal to 25, $\mathrm{T_{initial}}$ is varied to identify that value of $\mathrm{T_{initial}}$ when $E^{\mathrm{c}}_{\mathrm{R\,max}}$ and $E^{\mathrm{o}}_{\mathrm{R\,max}}$ are least. From Table VII, it is seen that corresponding to $\mathrm{T_{initial}}$ equal to 50 000 both $E^{\mathrm{c}}_{\mathrm{Ramx}}$ and $E^{\mathrm{o}}_{\mathrm{R\,max}}$ are least. Hence, with a seed equal to 25 and $\mathrm{T_{initial}}$ equal to 50000, TCF has been varied. From Table VIII, it is seen that for the TCF equal to 0.94, both $E^{\mathrm{c}}_{\mathrm{Ramx}}$ and $E^{\mathrm{o}}_{\mathrm{R\,max}}$ are least. Again, it has been reported earlier that for example 2, the convergence of the SAA has not been affected by its other parameters. Thus, from Table VII, it can be said that the SAA has converged to the values of the design parameters given in Table XII.

Similar studies have been carried for the HJA, the results of which are also presented in Table XII.

I. Merits of ANN-Aided SAA as an Optimization Tool for 3-D Electric-Field Optimization

The results of $E_{\mathrm{R\,max}}$ obtained from electric-field calculations were evaluated using 856 nodes on the electrode surfaces, 486 nodes on the insulator surfaces, and 2866 triangular boundary elements for example 1. Similar results were obtained using 975 nodes on the electrode surfaces, 330 nodes on the insulator surface, and the entire electrode-spacer arrangement discretized into 2400 triangular boundary surfaces for example 2. These optimized values were obtained by considering a large number of combinations of the above parameters and selecting the best among them.

Using a Pentium III 500-MHz PC with 128-MB random-access memory (RAM), the time required for the field calculation based on the Indirect BEM is 55 min for example 1 and 45 min for example 2. This includes the time for construction of the coefficient matrix and the time to solve the set of matrix equations.

In comparison, the total time required for the execution of the ANN aided SAA loop to produce the optimized values is 12 min for example 1 and 10 min for example 2 using the same PC. The execution time for the ANN-aided HJA for the two examples are 45 and 40 min, respectively.

Thus, a major saving in execution time can be achieved by coupling the SAA loop with a trained ANN as a cost function evaluator. Otherwise, the evaluation of the cost function through actual field calculation in every SAA step would require of the order of many hours to produce the final optimized values of the design parameters and the corresponding least $E_{\mathrm{R\,max}}$.

Another advantage of using an ANN-aided SAA is that the upper and lower bound of the control parameters can be modified at ease by varying the range of training data for the ANN.

This problem has also been tried with the GA. It has been observed that the GA converged exactly to the same solution space as that of the SAA. The difference is that the GA has converged in 6 min for example 1 while this time is 5 min for example 2. Thus, the GA has not substantially improved the execution time compared to the SAA.

TABLE XIV
TABLE FOR STATISTICAL ANALYSIS

E_{Rmax}	$x_{1\mathrm{mean}}$	σ_1	$n_1 = n_2$	$x_{2\mathrm{mean}}$	σ_2	z
Application Example 1						
$E^{0\mathrm{mx}}{}_{\mathrm{Rmax}}$	3.825	0.253	100	3.965	0.251	-1.97
$E^{0\mathrm{mn}}{}_{\mathrm{Rmax}}$	1.155	0.263	100	1.597	0.289	-5.95
$E^{0\mathrm{av}}{}_{\mathrm{Rmax}}$	2.997	0.325	100	3.215	0.327	-2.76
Application Example 2						
$E^{0\mathrm{mx}}{}_{\mathrm{Rmax}}$	9.240	0.203	100	9.560	0.218	-4.93
$E^{0\mathrm{mn}}{}_{\mathrm{Rmax}}$	7.89	0.153	100	8.025	0.163	-2.32
$E^{0\mathrm{av}}{}_{\mathrm{Rmax}}$	8.216	0.104	100	8.535	0.156	-6.26

Moreover, the results obtained from the SAA and the GA are compared statistically. For this purpose, the difference between the maximum values, minimum values, and average values of $E^{\mathrm{o}}_{\mathrm{R\,max}}$ obtained from the two optimization algorithms for a given value of seed have been estimated at a 95% degree of confidence. The principle for carrying this test of hypothesis is as follows:

If μ_1 and μ_2 are the values of the population means of the two independent random variables, then to estimate the equality of the population means

The null hypothesis is $H_0 : \mu_1 = \mu_2$. The alternative hypothesis is $H_1 : \mu_1 < \mu_2$. The test statistic is

$$z = \frac{\{x_{1\mathrm{mean}} - x_{2\mathrm{mean}}\}}{\left\{\frac{\sigma_1^2}{n_1} + \frac{\sigma_2^2}{n_2}\right\}^{1/2}}. \tag{4}$$

The critical region at 95% confidence interval is

$$z <= -1.645.$$

where $x_{i\mathrm{mean}}$, σ_i, and n_i are, respectively, the sample mean, population standard deviation, and sample size of the ith population ($i = 1, 2$). Here, each optimization algorithm has been trailed with 127 seeds; hence, the population size in each of the cases is 127. From each of these populations, a sample of size 100 was considered for this study. Again for this study, index 1 refers to the SAA, while index 2 refers to the GA. Table XIV presents the results for this statistical analysis.

From Table XIV, it is seen that the mean of the maximum value, the mean of the minimum value, and the average value of $E^{\mathrm{o}}_{\mathrm{Ramx}}$ (i.e E^{omx}, E^{omn}, and E^{oav}, respectively, lie in the critical region of the test statistic (i.e., in the critical region of z). Hence, it may be concluded that though both the SAA and the GA have converged to the same solution space but the former has statistically guaranteed convergence to the global optimum.

IX. CONCLUSION

The results presented were obtained with the help of PC-based software developed by the authors. The software implements electric-field calculations by the indirect BEM, ANN algorithm, and SAA. Two examples are provided where a trained ANN loop used for evaluation of the cost function results in reduction in computation time compared to evaluation of the cost function by field computation.

The degree of accuracy of the proposed method for obtaining optimized field distribution has also been verified. The results have been tested for statistical convergence of the SAA. The results of the proposed method show an acceptable degree of

accuracy that proves its ability to provide good solutions to the problems of optimizing electrode-spacer contours efficiently.

REFERENCES

[1] Y. Y. Hsu and C. C. Yang, "Design of artificial neural network for short term load forecasting. Part II: Multilayer feedforward network for peak load and valley load forecasting," *Proc. Inst. Elect. Eng. C*, vol. 138, no. 5, pp. 414–418, 1991.

[2] K. L. Ho, Y. Y. Hsu, and C. C. Yang, "Short term load forecasting using a multilayer neural network with an adaptive learning algorithm," *IEEE Trans. Power Syst.*, vol. 7, no. 1, pp. 141–149, Feb. 1992.

[3] N. Hosumi, T. Okamoto, and T. Imajo, "Discrimination of partial discharge patterns using a neural network," *IEEE Trans. Elect. Insul.*, vol. 27, no. 3, pp. 550–556, Jul. 1992.

[4] H. Singer and P. Grafoner, "Optimization of electrode and insulator contours," in *Proc. 2nd Int. Symp. HV Engineering*, Zürich, Switzerland, 1975, pp. 111–116.

[5] Z. Stih, "High voltage insulating system design by application of electrode and insulator contour optimization," *IEEE Trans. Elect. Insul.*, vol. EI-21, no. 4, pp. 579–584, Aug. 1986.

[6] M. Abdel-Salam and E. K. Stanek, "Optimizing field stress on HV insulators," *IEEE Trans. Elect. Insul.*, vol. EI-22, no. 1, pp. 47–56, Feb. 1987.

[7] S. Chakravorti and P. K. Mukherjee, "Application of artificial neural networks for optimization of electrode contour," *IEEE Trans. Dielect. Elect. Insul.*, vol. 1, pp. 254–264, Feb. 1994.

[8] K. Bhattacharya, S. Chakravorti, and P. K. Mukherjee, "An application of artificial neural network in the design of toroidal electrodes," *J. Inst. Eng. (India)*, pt. CP, vol. 76, pp. 14–20, 1995.

[9] ——, "Insulator contour optimization by artificial neural network," *IEEE Trans. Dielect. Elect. Insul.*, vol. 8, no. 2, pp. 157–161, Apr. 2001.

[10] P. K. Mukherjee, C. Trinitis, and H. Steinbigler, "Optimization of HV electrode systems by neural networks using a new learning method," *IEEE Trans. Dielect. Elect. Insul.*, vol. 3, no. 6, pp. 737–742, Dec. 1996.

[11] Z. Andjelic, B. Krstajic, S. Milojkovic, A. Blaszczyk, H. Steinbigler, and M. Wohlmuth, "Integral methods for the calculation of electric fields," in *Scientific Series Int. Bureau*, Germany: Forschungszentrum Jülich Gmbh, 1992, vol. 10.

[12] L. G. Christophorou and R. J. Burnt, "SF_6/N_2 mixtures, basic and HV insulation properties," *IEEE Trans. Dielect. Elect. Insul.*, vol. 2, no. 5, pp. 952–1002, Oct. 1995.

[13] S. Chakravorti and H. Steinbigler, "Electric field calculation including surface and volume resistivities by boundary element method," *J. Inst. Eng. (India)*, pt. El, vol. 78, pp. 17–23, 1997.

[14] S. Krikpatric, C. D. Gelatt, and M. P. Vecchi, "Optimization by simulated annealing," *Science*, vol. 220, pp. 671–680, 1983.

[15] M. P. Vecchi and S. Krikpatric, "Global wiring by simulated annealing," *IEEE Trans. Computer-Aided Design*, vol. CAD-2, no. 4, pp. 215–222, Oct. 1983.

[16] A. Corana, M. Marchesi, C. Martini, and S. Ridella, "Minimizing multimodal functions of continuous variables with the 'Simulated Annealing' algorithm," *ACM Trans. Math. Softw.*, vol. 13, pp. 262–280, 1987.

[17] D. Vanderbilt and S. G. Louie, "A Monte Carlo simulated annealing approach to optimization over continuous variables," *J. Comput. Phys.*, vol. 56, pp. 259–271, 1984.

[18] R. H. J. M. Otten and L. P. P. P. van Ginneken, *The Annealing Algorithm*. Norwell, MA: Kluwer, 1989.

[19] S. Krikpatric, "Optimization by simulated annealing: Quantitative studies," *J. Stat. Phys.*, vol. 34, pp. 975–986, 1984.

[20] L. Nolle, D. A. Amstrong, A. A. Hopgood, and J. A. Ware, "Simulated annealing and genetic algorithms applied to finishing mill optimization for hot rolling of wide steel strip," *Int. J. Knowledge-Based Intelligent Engineering Systems*, vol. 6, no. 2, pp. 104–111, 2002.

[21] R. Hooke and T. A. Jeeves, "'Direct Search'": Solution of numerical and statistical problems," *J. Assoc. Comput. Mach.*, vol. 8, no. 2, pp. 212–229, 1961.

Abhijit Lahiri received the physics degree (Hons.) from the University of Calcutta, Kolkata, India, the M.Tech. degree in industrial electrical systems from Burdwan University, Burdwan, India, and the Ph.D. degree from Jadavpur University, Kolkata, India.

Currently, he is a Full-Time Faculty Member in the Department of Electrical Engineering, Calcutta Institute of Engineering and Management, Kolkata, India. His research interests include numerical electrostatic-field computation, computer-aided design for the optimization of insulation systems, and application of artificial intelligence in high-voltage systems.

Sivaji Chakravorti (M'90–SM'00) received the B.E.E., M.E.E., and Ph.D. degrees from Jadavpur University, Kolkata, India, in 1983, 1985, and 1993, respectively.

Currently, he is a Professor of Electrical Engineering in the Electrical Engineering Department, Jadavpur University. He was a Humboldt Research Fellow with the Technical University, Munich, Germany, in 1995–1996 and 1999, respectively. He was a Development Engineer with Siemens AG, Berlin, Germany, in 1998. He was also a Humboldt Research Fellow with ABB Corporate Research, Ladenburg, Germany, in 2002. In 2003, he was a U.S. National Science Foundation Guest Scientist with Virginia Polytechnic Institute and State University, Blacksburg. He has published about 70 research papers, has authored a book, and edited two books. His research interests are numerical field computation, computer-aided design and optimization of insulation system, application of artificial intelligence in high-voltage systems, and lifelong learning techniques.